Power flow from a dipole emitter near an optical antenna

Kevin C. Y. Huang,[1,*] **Young Chul Jun,**[1,2] **Min-Kyo Seo,**[1,3] **and Mark L. Brongersma**[1]

[1]*Geballe Laboratory for Advanced Materials, Stanford University, Stanford, California 94305, USA*
[2]*Sandia National Laboratories, Albuquerque, New Mexico 87185, USA*
[3]*Korea Advanced Institute of Science and Technology, Daejeong, Korea*
[*]*khu834@stanford.edu*

Abstract: Current methods to calculate the emission enhancement of a quantum emitter coupled to an optical antenna of arbitrary geometry rely on analyzing the *total* Poynting vector power flow out of the emitter or the dyadic Green functions from full-field numerical simulations. Unfortunately, these methods do not provide information regarding the nature of the dominant energy decay pathways. We present a new approach that allows for a rigorous separation, quantification, and visualization of the emitter output power flow captured by an antenna and the subsequent reradiation power flow to the far field. Such analysis reveals unprecedented details of the emitter/ antenna coupling mechanisms and thus opens up new design strategies for strongly interacting emitter/ antenna systems used in sensing, active plasmonics and metamaterials, and quantum optics.

OCIS codes: (240.6680) Surface plasmons; (140.4780) Optical resonators; (270.5580) Quantum electrodynamics; (260.3910) Metal optics; (260.2510) Fluorescence.

References and links

1. E. M. Purcell, "Spontaneous emission probabilities at radio frequencies," Phy. Rev. **69**, 681 (1946).
2. P. R. Berman, *Cavity Quantum Electrodynamics* (Academic Press, 1994).
3. Y. C. Jun, R. D. Kekatpure, J. S. White, and M. L. Brongersma, "Nonresonant enhancement of spontaneous emission in metal-dielectric-metal plasmon waveguide structures," Phy. Rev. B **78**, 153111 (2008).
4. R. Esteban, T. V. Teperik, and J. J. Greffet, "Optical patch antennas for single photon emission using surface plasmonic resonances," Phy. Rev. Lett. **104**, 026802 (2010).
5. P. Bharadwaj, B. Deutsch, and L. Novotny, "Optical antennas," Adv. Opt. Photon. **1**, 438–483 (2009).
6. M. V. Bashevoy, V. A. Fedotov, and N. I. Zheludev, "Optical whirlpool on an absorbing metallic nanoparticle," Opt. Express **13**, 8372–8379 (2005).
7. T. H. Taminiau, F. D. Stefani, and N. F. van Hulst, "Single emitters coupled to plasmonic nano-antennas: angular emission and collection efficiency," New J. Phys. **10**, 105005 (2008).
8. R. M. Bakker, V. P. Drachev, Z. Liu, H. Yuang, R. H. Pedersen, A. Boltasseva, J. Chen, J. Irudayaraj, A. V. Kildishev, and V. M. Shalaev, "Nanoantenna array-induced fluorescence enhancement and reduced lifetimes," New J. Phys. **10**, 125022 (2008).
9. D. E. Chang, A. S. Sorensen, P. R. Hemmer, and M. D. Lukin, "Strong coupling of single emitters to surface plasmon," Phy. Rev. B **76**, 035420 (2007).
10. T. H. Taminiau, F. D. Stefani, F. B. Segerink, and N. F. van Hulst, "Optical antennas direct single-molecule emission," Nat. Photonics **2**, 234–237 (2008).
11. J. N. Farahani, H. Eisler, D. W. Pohl, M. Pavius, P. Fluckiger, P. Gasser, and B. Hecht, "Bow-tie optical antenna probes for single-emitter scanning near-field optical microscopy," Nanotechnology **18**, 125506 (2007).
12. L. Rogobete, F. Kaminski, M. Agio, and V. Sandoghdar, "Design of plasmonic nanoantennae for enhancing spontaneous emission," Opt. Lett. **32**, 1623–1625 (2007).

#150873 - $15.00 USD Received 13 Jul 2011; revised 3 Aug 2011; accepted 3 Aug 2011; published 15 Sep 2011

13. S. Kuhn, U. Hakanson, L. Rogobete, and V. Sandoghdar, "Enhancement of single-molecule fluorescence using a gold nanoparticle as an optical nanoantenna," Phy. Rev. Lett. **97**, 017402 (2006).
14. A. G. Curto, G. Volpe, T. H. Taminiau, M. P. Kreuzer, R. Quidant, and N. F. van Hulst, "Unidirectional emission of a quantum dot coupled to a nanoantenna," Science **329**, 930–933 (2010).
15. P. G. Etchegoin and E. C. L. Ru, "Multipolar emission in the vicinity of metallic nanostructures," J. Phys.: Condens. Matter **18**, 1175–1188 (2006).
16. Y. C. Jun, K. C. Y. Huang, and M. L. Brongersma, "Plasmonic beaming and active control over fluorescent emission," Nat. Commun. **2**, 283 (2011).
17. A. F. Koenderink, "On the use of purcell factors for plasmon antennas," Opt. Lett. **35**, 4208–4210 (2010).
18. H. Chew, "Radiation and lifetimes of atoms inside dielectric particles," Phy. Rev. A **38**, 3410–3416 (1988).
19. R. R. Chance, A. Prock, and R. Silbey, *Molecular Fluorescence and Energy Transfer Near Interfaces* (Wiley, 1978), Vol. 37.
20. L. Novotny and B. Hecht, *Principles of Nano-optics* (Cambridge Univ. Press, 2006).
21. T. H. Taminiau, F. D. Stefani, and N. F. van Hulst, "Optical nanorod antennas modeled as cavities for dipolar emitters: optical nanorod antennas modeled as cavities for dipolar emitters: evolution of sub- and super-radiant mode," Nano Lett. **11**, 1020–1024 (2011).
22. C. F. Bohren and D. R. Huffman, *Absorption and Scattering of Light by Small Particles* (Wiley, 1983).
23. C. F. Bohren, "How can a particle absorb more than the light incident on it?" Am. J. Phys. **51**, 323–327 (1983).
24. H. T. Miyazaki and Y. Kurokawa, "How can a resonant nanogap enhnace optical fields by many orders of magnitude?" IEEE J. Sel. Top. Quantum Electron. **14**, 1565–1576 (2008).
25. E. S. Barnard, J. S. White, A. Chandran, and M. L. Brongersma, "Spectral properties of plasmonic resonator antennas," Opt. Express **16**, 16529–16537 (2008).
26. G. D. Valle, T. Sondergaard, and S. I. Bozhevolnyi, "Plasmon-polariton nano-strip resonators: from visible to infra-red," Opt. Express **16**, 6867–6876 (2008).
27. A. Taflove and S. C. Hagness, *Computational Electrodynamics: The Finite-Difference Time-Domain Method* (Artech House, 2005), 3rd ed.

1. Introduction

In 1946, Purcell demonstrated that the emission properties of a quantum emitter which is coherently coupled to its environment can be significantly modified [1]. The ability to engineer radiative processes has inspired many fundamental physics studies and propelled the design and realization of a myriad of practical photonic devices [2]. With the emergence of plasmonics and metamaterials, researchers have now gained an interest in understanding the coupling of quantum emitters to a great diversity of nanoscale optical antennas capable of channeling the energy flow into the far field [3–16] thus modifying the efficiency, modulation speed, angular emission distribution, and the polarization behavior of the optical emission.

As opposed to high-Q dielectric cavities, inside which the emitter interacts predominantly with modes having negligible radiation leakage, the coupling of an emitter to a low-Q antenna cannot be accurately characterized by the ratio between the quality factor (Q) and the mode volume (V) [17]. This is because optical antennas support a continuum of radiation, guided and evanescent higher-order modes, each of which has a distinct Q/V and all contribute strongly to the enhanced local density of optical states (LDOS). The exact mode coupling strength between an emitter and objects of spherical [18], cylindrical [9] or planar geometries [19] can be obtained using an analytical normal mode expansion. However, the coupling of emitters to an optical antenna of complex geometry must be solved with numerical methods. This allows one to extract the total decay rate enhancement of the dipole but provides no information regarding the details of the emitter decay channels. The inability to solve for the electromagnetic response of the antenna system excited by a dipole in terms of an intuitive normal mode framework severely limits further understanding and engineering of the emission enhancement process regardless of the choice of the physical pictures ranging from LDOS, Poynting vector power flow, power dissipation of a damped driven harmonic oscillator [20] or a point-like current source driving a nearby optical antenna with an effective radiation resistance [5, 21].

In this letter, we show that the energy decay pathways near an antenna can be rigorously analyzed to provide new insights into the role of the antenna in controlling the decay rate and

#150873 - $15.00 USD Received 13 Jul 2011; revised 3 Aug 2011; accepted 3 Aug 2011; published 15 Sep 2011

far-field emission properties. To this end, we separate the total Poynting vector into components that show the power radiated by the emitter and the power scattered by the antenna. In contrast to the common analysis of the total Poynting vector, this procedure reveals how the antenna enhances and controls the emission by providing new decay channels via which it effectively captures and then redistributes the emission from a dipole source.

2. Poynting's theory for spontaneous emission enhancement

The power flow analysis described in this Letter is inspired by a methodology proposed by Bohren [22, 23], Miyazaki and Kurokawa [24]. They visualized the interaction of planewaves with metallic nanostructures to gain important physical intuition about absorption and scattering processes. In this Letter, we extended their method to describe and visualize the interaction between a dipole emitter and a nearby optical antenna. It is this interaction (back-action of the antenna on the source) that results in the emergence of new decay channels and a concomitant enhancement in the emission.

Our analysis starts by separating the total Poynting vector $\vec{S}_{tot}$ into the emitter output $\vec{S}_{out}$ and antenna scattering $\vec{S}_{scat}$. To this end, we first consider a dipole emitter in a homogeneous medium that produces the incident electric and magnetic fields ($\vec{E}_{inc}$ and $\vec{H}_{inc}$). When an optical antenna is introduced, we define the total resulting electric and magnetic fields ($\vec{E}_{tot}$ and $\vec{H}_{tot}$). A simple subtraction of the incident fields from the total fields gives the scattered fields: $\vec{E}_{scat}(\vec{r}) = \vec{E}_{tot}(\vec{r}) - \vec{E}_{inc}(\vec{r})$, and $\vec{H}_{scat}(\vec{r}) = \vec{H}_{tot}(\vec{r}) - \vec{H}_{inc}(\vec{r})$. These are the fields which arise from regions where the dielectric function is perturbed from the original homogeneous medium. The total time-averaged Poynting vector at each spatial location is given by $\vec{S}_{tot}(\vec{r}) = \frac{1}{2}\Re\{\vec{E}_{tot}(\vec{r}) \times \vec{H}^*_{tot}(\vec{r})\}$. We can elect to write $\vec{S}_{tot}$ in terms of the incident and scattered fields omitting the $\vec{r}$ dependence from now on for brevity: $\vec{S}_{tot} = \frac{1}{2}\Re\{\vec{E}_{inc} \times \vec{H}^*_{inc} + \vec{E}_{inc} \times \vec{H}^*_{scat} + \vec{E}_{scat} \times \vec{H}^*_{inc} + \vec{E}_{scat} \times \vec{H}^*_{scat}\}$ For reasons that will become clear, we define the first three terms in the expansion of $\vec{S}_{tot}$ as the emitter output Poynting vector $\vec{S}_{out}$ and the last term as the antenna scattering Poynting vector $\vec{S}_{scat}$:

$$\begin{aligned} \vec{S}_{out} &= \frac{1}{2}\Re\{\vec{E}_{inc} \times \vec{H}^*_{inc} + \vec{E}_{inc} \times \vec{H}^*_{scat} + \vec{E}_{scat} \times \vec{H}^*_{inc}\} \\ \vec{S}_{scat} &= \frac{1}{2}\Re\{\vec{E}_{scat} \times \vec{H}^*_{scat}\} \end{aligned} \tag{1}$$

The first term $\vec{S}_{inc} = \frac{1}{2}\Re\{\vec{E}_{inc} \times \vec{H}^*_{inc}\}$ simply describes the power flow of the emission in the homogenous medium. The last term $\vec{E}_{scat} \times \vec{H}^*_{scat}$ is the power flow directed away from the antenna. The physical meaning of the two cross terms ($\vec{S}_{cross}(\vec{r}) = \frac{1}{2}\Re\{\vec{E}_{inc}(\vec{r}) \times \vec{H}^*_{scat} + \vec{E}_{scat} \times \vec{H}^*_{inc}\}$) can be understood by examining the definition of spontaneous emission enhancement

$$\frac{P_{tot}}{P_{inc}} = \frac{\oint_A \vec{S}_{tot} \cdot \hat{n}\, dA}{\oint_A \vec{S}_{inc} \cdot \hat{n}\, dA} = 1 + \frac{\oint_A \vec{S}_{cross} \cdot \hat{n}\, dA}{\oint_A \vec{S}_{inc} \cdot \hat{n}\, dA} \tag{2}$$

where A is an arbitrary closed surface which fully encloses only the emitter and $\hat{n}$ is the unit vector normal to the surface A. This simplification results from the fact that the scatterer is outside of the closed surface A, therefore the scattered power which originates from the antenna $\vec{S}_{scat}$ does not contribute to the closed-loop integral over $\vec{S}_{tot}$. By comparing (2) to the classical emission enhancement equation [20], it is clear that the coherent interaction between the incident and scattered fields gives rise to the modified energy decay pathways responsible for the emission enhancement.

#150873 - $15.00 USD Received 13 Jul 2011; revised 3 Aug 2011; accepted 3 Aug 2011; published 15 Sep 2011

3. Emitter near a plasmonic resonator antenna

We consider an emitter near a plasmonic resonator antenna (PRA), a model system consisting of a thin metallic stripe with wavelength-scale dimensions [25]. Such a structure acts as a low-Q resonator by supporting integer number of half-wavelength resonances for short-range surface-plasmon-polaritons (SR-SPPs) [25, 26]. Due to the strong field enhancements at the ends of the PRA, many have explored their properties to enhance fluorescence from emitters [5,8,9,14,21]. In contrast to these studies which focus on the total emission near an antenna, our method describes the antenna as serving two separate functions, first, the transfer of the emitter energy to the antenna, and second, the out-coupling of the captured energy with a controlled angular distribution.

We performed finite-difference time-domain (FDTD) simulations [27] in the two-dimensional (2D) transverse magnetic polarization of an electric dipole oscillating in-plane at 850nm free space wavelength located near a 20nm thick Ag stripe of varying widths surrounded by vacuum. We simulated two separate scenarios: one with and one without the Ag PRA to obtain the total and incident complex vector fields respectively. The total and incident fields were then used to calculate $\vec{S}_{out}(\vec{r})$ and $\vec{S}_{scat}(\vec{r})$ in the presence of the antenna according to (1). Unity quantum efficiency is assumed for the emitter.

Figure 1 corresponds to the case where a vertically polarized emitter is placed 20nm underneath the end of a horizontal, 246nm wide PRA. Figures 1(a) and 1(b) is a comparison between (a) the first order SR-SPP eigenmode of the PRA solved using COMSOL Multiphysics (in-plane propagation) and (b), the magnitude of the scattered electric field excited by the emitter calculated in FDTD. These two figures show that the emitter not only couples to the SR-SPP resonance of the PRA, higher-order localized modes are also strongly excited, resulting in a much higher field intensity near the end of the PRA closest to the emitter. For this reason, attempts to analyze the Purcell factor based on a single (or several) eigenmode Q/V ratio is only approximately correct, while direct numerical analysis of the total decay rate (power flow, Green's function or LDOS) does not yield information regarding the dominant decay paths since the emitter is coupled to a large number of channels, all of which contribute to the enhanced emission.

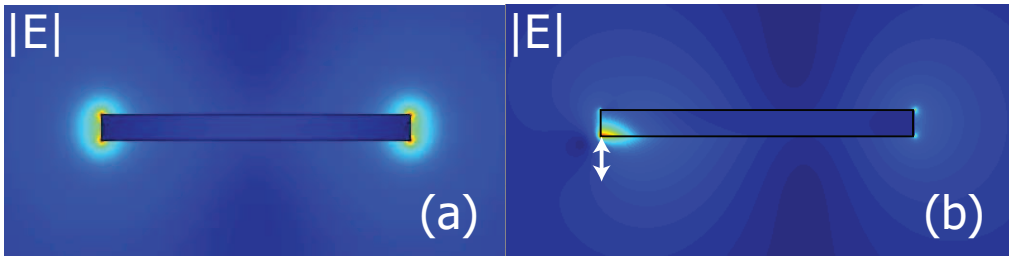

Fig. 1. (a) Linear plot of the magnitude of the electric field for the lowest order eigenmode for a 20nm thick Ag PRA in air. (b) Linear plot of the magnitude of the scattered electric field due to the excitation by a vertically oriented electric dipole placed 20nm beneath the left end of a Ag PRA .

First we show how qualitative and quantitative information can be obtained on the antenna's ability to redirect emission. We calculated the emitter power transfer to the antenna P_{transf} ($\vec{S}_{out}$ integrated around the PRA, this quantity is negative as the power is flowing inwards) and the power emitted to free space radiation modes P_{fs} ($\vec{S}_{out}$ integrated around both the PRA and the emitter, this quantity is positive as the power is flowing outwards) as a function of the emitter/

#150873 - $15.00 USD Received 13 Jul 2011; revised 3 Aug 2011; accepted 3 Aug 2011; published 15 Sep 2011

PRA separation. Note that P_{fs} is different from the dipole emission in free space as it includes interference of the antenna scattered fields, more detailed explanation of the physical meaning of P_{fs} will be given below. This orthogonal end-coupled configuration (Fig. 2 inset) is particularly instructive because the emission from the dipole and the antenna do not interfere in the far field at 0°and 90°. This simplifies the comparison between the relative contributions of P_{transf} and P_{fs} to the far-field emission. We performed near-to-far-field transformation (NTFF) to obtain the total far-field emission patterns for several emitter/ PRA separations. By comparing the power per radian ratio of the total emission at 90°and 0°with the ratio of $|P_{transf}|$ to P_{fs} as a function of separation (Fig. 2), we see that an effective coupling of the emitter to the antenna (i.e. large $|P_{transf}|/P_{fs}$ ratio) enables the antenna to redirect the emission. Previous models do not provide quantitative information on the coupled power to the antenna or assumed perfect coupling.

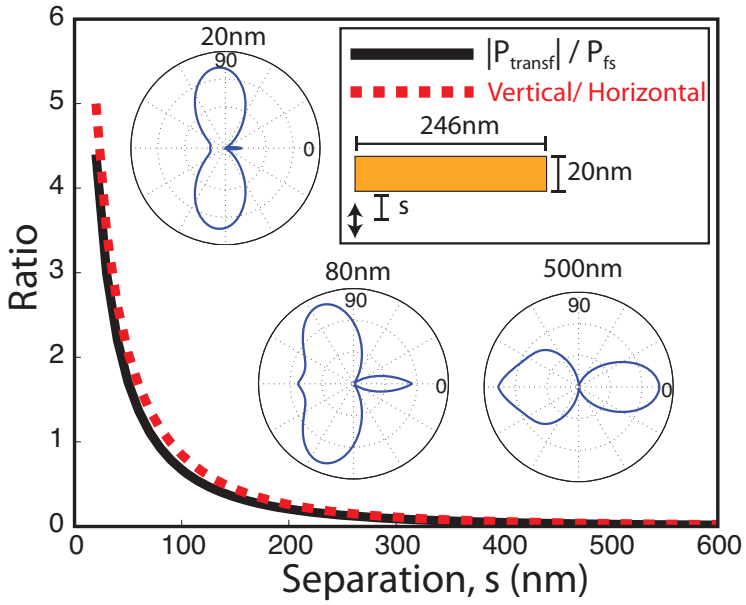

Fig. 2. Ratio of antenna-directed emission to direct free space emission of a vertically oriented dipole placed underneath the edge of a 20nm thick by 246nm wide horizontal PRA as a function of separation. Ratio of PRA transfer power flow to free space emission $|P_{transf}|/P_{fs}$ (solid black). Ratio of far-field radiated power per radian at 90°and 0°(red dashed). Far-field emission pattern for separations of 20, 80 and 500nm are shown as well.

Next, we quantify the antenna power efficiency by integrating $\vec{S}_{scat}$ around the PRA to obtain the scattered power P_{scat}. As opposed to the conventional calculation of antenna efficiency which takes the ratio of total radiated power P_{rad} to total emitted power P_{tot} (total efficiency), dividing P_{scat} by $|P_{transf}|$ quantifies the fraction of the power transferred to the PRA which is subsequently reradiated. The difference between the power transfer to the antenna and power leaving the antenna is the non-radiated power ($P_{nrad} = P_{transf} + P_{scat}$) or heat deposited in the antenna (has a negative sign). Figure 3 compares the total efficiency and PRA efficiency as a function of PRA width for a vertical emitter placed 20nm beneath the end of a PRA (inset) . At short widths, the total efficiency (solid black) is close to 1 which could mislead one to believe that short PRAs ($<$ 100nm) are efficient. However, looking at the red dashed curve, we see that

#150873 - $15.00 USD Received 13 Jul 2011; revised 3 Aug 2011; accepted 3 Aug 2011; published 15 Sep 2011

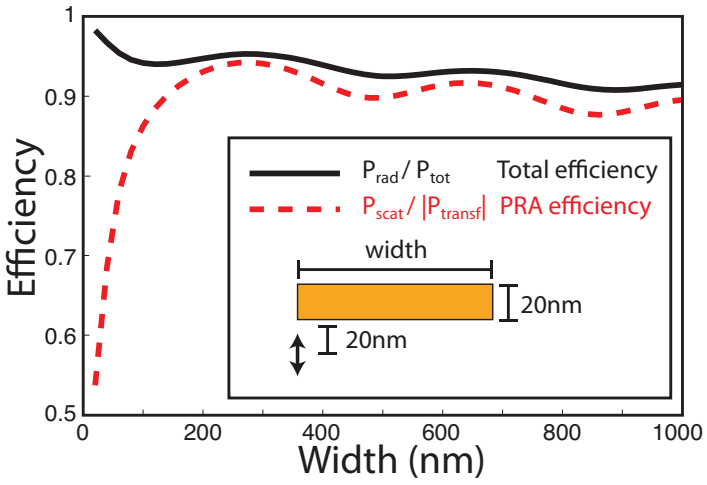

Fig. 3. Total radiative efficiency P_{rad}/P_{tot} (solid black) and PRA radiative efficiency $P_{scat}/|P_{transf}|$ (red dashed) as a function of the PRA width.

this is not the case as the PRA efficiency drops sharply (red dashed). This discrepancy arises because the majority of the emission is not captured by ineffective, short antennas.

One of the most critical consequences of the power flow analysis is the separation of the decay channels which contribute to the emission enhancements. Figure 4 shows the emission rate enhancement of each channel (normalized to the emission rate in free space) as an emitter centered below a PRA is brought into close proximity of the antenna. Conventionally, only the total (solid black) and its non-radiative (orange thick dash dot) and radiative (green thick dotted) components are obtained by integrating $\vec{S}_{tot}$ around closed-surfaces enclosing the emitter, the PRA, or the emitter/ PRA together. As expected, at large separation, the dipole emission is mostly radiative while reducing the separation enhances the total emission at the cost of increased non-radiative losses in the metal. However, in order to quantify how much of the far-field emission is redirected by the PRA, one must distinguish the contribution of the direct dipole free space radiation and the PRA reradiation to the total radiated power, which cannot be obtained by analyzing $\vec{S}_{tot}$. To identify their respective contributions, we made a different decomposition of the total emission in terms of $|P_{transf}|$ and P_{fs}, which is enabled by our power flow calculations. The emission captured by the antenna quantified by $|P_{transf}|$ monotonically increases with decreasing emitter/antenna separation (blue thin dotted). In contrast, the direct free space radiation quantified by P_{fs} oscillates around a value of 1 (red thin dash dot). This is an indication that the emission directed into the PRA is governed by near-field coupling mechanisms while the free space radiation is determined by the interference of the dipole incident fields and the antenna scattered fields (phase coupling).

The above results strongly support our interpretation that P_{transf} represents the large wavevector (confined modes) decay channels introduced by the PRA and P_{fs} represents the interference of low wavevector radiation modes. In waveguide language, P_{transf} is power coupled into confined or guided modes (below the light line) which can only radiate out (P_{scat}) after a change in wavevector. P_{fs} is the power emitted directly into propagating modes in the surrounding medium (above the light line). For typical nm scale emitter/ antenna separations, it is often tacitly (and wrongly) assumed that all of the emission flows via the antenna, however, detailed decay channel analysis shows that free space emission may be substantial and must be

#150873 - $15.00 USD Received 13 Jul 2011; revised 3 Aug 2011; accepted 3 Aug 2011; published 15 Sep 2011

carefully considered.

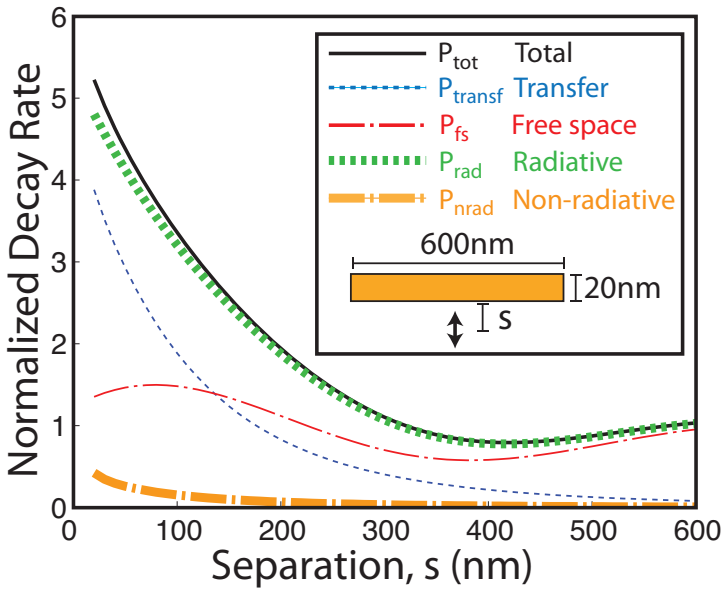

Fig. 4. Decay channel coupling strengths of a vertically oriented dipole placed underneath the center of a 20nm thick 600nm wide horizontal PRA as a function of separation (inset). Total decay enhancement P_{tot} (solid black), radiative decay enhancement P_{rad} (thick green dotted), transferred power to the PRA $|P_{transf}|$ (thin blue dotted), free space radiation mode emission P_{fs} (thin red dash dot) and non-radiative decay enhancement P_{nrad} (thick orange dash dot).

Finally, to visually illustrate the difference in the types of information which can be obtained from the traditional analysis of $\vec{S}_{tot}$ and our proposed study of $\vec{S}_{out}$ and $\vec{S}_{scat}$, we plotted the magnitudes of the time-averaged Poynting vector in log scale with overlaid vector field streamlines that visualize the direction and magnitude of the local power flows. The streamlines are spaced such that each represents a fixed amount of power flux and is tangential to the underlying vector fields . They satisfy the equation $\frac{\vec{S}_x}{dx} = \frac{\vec{S}_y}{dy}$. Figures 5(a)–5(c) show the visualization of $\vec{S}_{tot}$, $\vec{S}_{out}$ and $\vec{S}_{scat}$ for a vertical dipole placed 20nm beneath the PRA. Since $\vec{S}_{tot} = \vec{S}_{out} + \vec{S}_{scat}$, by separating the power flowing into ($\vec{S}_{out}$) and out of ($\vec{S}_{scat}$) the PRA, we can clearly identify the fraction of the emitted power flow lines captured by the PRA (P_{transf} colored red in Fig. 5(b)). We also see how the antenna subsequently reradiates the power in a quadrupolar fashion that is characteristic of an antenna that is about one surface plasmon wavelength wide (Fig. 5(c)). Furthermore, the flow lines not directed into the PRA represents substantial emission from the dipole into free space modes (P_{fs} Fig. 5(b) black lines). These important coupling information cannot be extracted from Fig. 5(a) which does not show how the emitted power flows via the PRA to the far field.

This is the first time to our knowledge that the emission of a dipole and the scattering from a nearby optical antenna is separately analyzed. Although the separation of incident and scattered fields is well-known in the analysis of planewave illumination of scatterers, this type of analysis has never been applied to study emitter/ scatterer systems and the relation between the Poynting vector cross terms and spontaneous emission enhancement has not been established. As a final

#150873 - $15.00 USD Received 13 Jul 2011; revised 3 Aug 2011; accepted 3 Aug 2011; published 15 Sep 2011

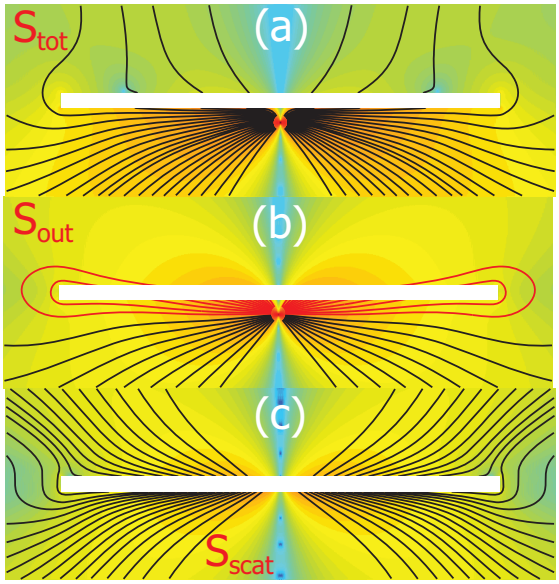

Fig. 5. Visualizations of the emission properties of a vertically oriented dipole placed 20nm underneath the center of a 20nm thick 600nm wide horizontal PRA. (a) Log plot of the magnitude of total Poynting vector $\vec{S}_{tot}$. (b) Log plot of the magnitude of emitter output Poynting vector $\vec{S}_{out}$. (c) Log plot of the magnitude of PRA scattering Poynting vector $\vec{S}_{scat}$.

note, we would like to point out that although all the examples above are the results of 2D simulations for ease of demonstration and visualization, the described power flow analysis and field computations are equally applicable in 3D. The derivation of (2) is based purely on power conservation thus the closed-loop integral can be surface or line integrals and is valid provided that the integration completely encloses the dipole emitter. The exact value of the spontaneous emission enhancement calculated will be different in 2D and 3D, however, the behavior of the dipole/ antenna system in the symmetric 2D plane is the same.

4. Conclusions

The presented results demonstrate that our proposed framework is ideally suited to quantitatively analyze the coupling of an emitter to an antenna, which is a non-trivial problem typically requiring a-priori knowledge of the dominant excited modes for highly symmetric structures [9, 18, 19] or simplified for more complex geometries [21]. We showed that the separation of total Poynting vector $\vec{S}_{tot}$ into the emitter output $\vec{S}_{out}$ and antenna scattering $\vec{S}_{scat}$ enables direct visualization and quantification of the power transfer from the source to the antenna and the subsequent reradiation to the far field. Simple power conservation considerations then lead to an accurate calculation of the antenna efficiency, which previously could only be estimated from the heat deposition in the antenna and by assuming that all of the radiated power flowed through the antenna. Application of power flow coupling efficiency analysis to experimental demonstrations of antenna-directed emitter radiation [8, 10, 13, 14] taking into account substrate effects and other non-idealities will further the understanding of measured results and provide guidelines to improve the design of strongly interacting emitter/ antenna systems for fundamental quantum electrodynamics studies and applications in sensing, active metamaterials and

#150873 - $15.00 USD Received 13 Jul 2011; revised 3 Aug 2011; accepted 3 Aug 2011; published 15 Sep 2011

power-efficient broadband optical sources.

Acknowledgments

We acknowledge funding support from the Air Force Office of Scientific Research (G. Pomrenke; grant no. FA9550-10-1-0264). Kevin C. Y. Huang would like to acknowledge funding support by the National Science Foundation Graduate Research Fellowship Program and Min-Kyo Seo acknowledges support from a National Research Foundation of Korea Grant funded by the Korean Government [NRF-2009-352-C00038]. We would like to thank Dr. Edward S. Barnard and Prof. Shanhui Fan for helpful discussions.

#150873 - $15.00 USD Received 13 Jul 2011; revised 3 Aug 2011; accepted 3 Aug 2011; published 15 Sep 2011